International Journal of Energy Research

INTERNATIONAL JOURNAL OF ENERGY RESEARCH
Int. J. Energy Res. 2015; **39**:128–139
Published online 26 June 2014 in Wiley Online Library (wileyonlinelibrary.com). DOI: 10.1002/er.3229

Synthesis and characterization of Pt-CMK-3 hybrid nanocomposite for hydrogen storage

Juliana M. Juárez, Marcos B. Gómez Costa and Oscar A. Anunziata*,†

Centro de Investigación en Nanociencia y Nanotecnologia (NANOTEC), Facultad Regional Córdoba, Universidad Tecnológica Nacional, Maestro López y Cruz Roja Argentina, 5016, Córdoba, Argentina

SUMMARY

The nanometric carbon CMK-3 modified with Pt was synthesized and applied as a reservoir for hydrogen uptake. We found that the newly synthesized hybrid composites exhibited significantly enhanced H_2 storage. The approach that we have followed includes synthesis of nanostructures with the experimental study of its adsorption capacity and storage properties. In summary, we have shown that CMK-3 ordered porous carbon modified with Pt nanoclusters is a promising material for hydrogen uptake. The samples were characterized by X-ray diffraction, N_2 isotherms, X-ray photoelectron spectra and transmission electron microscopy. The nanoparticles of Pt (~1.7 nm) incorporated onto the nanostructured carbon CMK-3 showed higher hydrogen uptake at low and high pressures (3.3 wt% of H_2 sorption at 10 bar and 77 K) than CMK-3. Copyright © 2014 John Wiley & Sons, Ltd.

KEY WORDS

hybrid nanocomposite; Pt-CMK-3; CMK-3; hydrogen storage

Correspondence

*Oscar A. Anunziata, Centro de Investigación en Nanociencia y Nanotecnologia (NANOTEC), Facultad Regional Córdoba, Universidad Tecnológica Nacional, Maestro López y Cruz Roja Argentina, 5016, Córdoba, Argentina.
†E-mail: oanunziata@scdt.frc.utn.edu.ar

Received 2 May 2014; Revised 27 May 2014; Accepted 27 May 2014

1. INTRODUCTION

Hydrogen is an alternative energy source of clean fuel and other industrial applications [1], can operate fuel cells and internal combustions engines [2], and is an alternative for non-renewable energy sources like oil [3].

The biggest challenge for hydrogen economy is the development of a viable storage system for hydrogen and has been recognized as an ideal energy carrier because it is easily produced from renewable energy sources and contains higher chemical energy per mass than hydrocarbon fuels [4].

In the past decades, hydrogen storage and transportation has been the major difficult in the hydrogen technology. The method of storing as compressed hydrogen or liquefied hydrogen is inappropriate for wide application because of its low storage density or high cost. Chemisorption of hydrogen in the form of metals or complex hydrides is an attractive method, but these materials are relatively expensive [4].

Physisorption of hydrogen on carbon-based nanomaterials or other porous materials have attracted greatly scientific interests. Porous carbons with well-ordered pore systems offered great potential in hydrogen storage [5–8].

Metal organic frameworks (MOFs) are very promising candidates in the field of gas separation and storage. A large portion of voids generated in MOFs usually remains unutilized for hydrogen storage because of weak interactions between the walls of MOFs and H_2 molecules. Saha and Deng [9] synthesized mixed crystals of MOF-5 and MOF-177 in order to determined hydrogen adsorption at hydrogen pressure up to 1.05 bar and different temperatures (77, 194.5, and 298 K).

Klyamkin *et al.* [10] synthesized porous chromium (III) oxoterphthalate MIL-101 and hybrid MIL-101/Pt/C composite materials. The hydrogen adsorption properties of porous materials were investigated at pressures up to 1000 bar. Hydrogen sorption capacity increases gradually with pressure and reaches 1.5 wt% instead of maximum 0.4 wt% for the pristine MIL-101.

Moussa *et al.* [11] studied boron-based hydrides for chemical hydrogen storage and concluded that boron-based hydrides have a significant potential in chemical hydrogen storage, but their implementation depends on the recyclability of the solid by-products.

Liang *et al.* [12] published unique properties of graphene and graphene-based materials in clean energy-related devices.

Copyright © 2014 John Wiley & Sons, Ltd.

Many activated and templated carbons with high-surface area exhibit potential for storing molecular hydrogen [4,13–15]. Nanostructured carbons are among the major candidates of physisorption for their lightweight, abundant natural precursors, and low cost. The activated carbons have been reported to have relatively high hydrogen storage capacity at 77 K [13,14], but the pore size distribution is generally wide, and more than half of the total porous volumes come from macropores, which contribute less to the uptake of hydrogen. Despite the fact that the carbon nanotubes and carbon nanofibers (CNFs) have been studied as hydrogen storage materials [15–21], there are still disputes about their capacities of hydrogen adsorption. Moreover, the carbon activation has also been reported to be useful for improving the pore structure and increasing the hydrogen uptake in new nanostructured carbon materials such as single-wall nanotubes and CNFs. Thus, the activation of the ordered porous carbon is desirable for getting a higher hydrogen uptake. The amounts of hydrogen adsorbed at atmospheric pressure on single-wall nanotubes reach approximately 0.01 wt% at 298 K and 1 wt% at 77 K [22], and H_2 sorption on CNF activated with KOH and CO_2 is between 0.05 and 0.35 wt% [23].

The carbons were obtained via the template method, which involved the introduction of suitable carbon precursors into the ordered pores of the template followed by carbonization and finally removal of the template [24–26]. These carbon materials usually have large specific surface areas and high pore volumes, which are useful for effective physisorption of H_2. Besides, the ordered networks may provide fast transportation in the materials, a noticeable volume of micropores can efficiently adsorb hydrogen, and the microporosity and the mesoporosity can be adjusted by changing the template, the carbon precursor, and the amount of carbon infiltrated in the template [5].

Hydrogen storage measurements on peels formed from powdered carbide-derived carbons mixed with polytetrafluorethylene were presented by Singer *et al*. [27]. Poirier *et al*. [28] studied hydrogen storage on CNFs and intercalated and exfoliated carbon materials. Giraudet *et al*. [29] studied the hydrogen adsorption on ordered mesoporous carbons (OMCs) doped with nickel nanoparticles.

Platinum and platinum alloys are used as catalysts for fuel oxidation and oxygen reduction reactions, and the usage of expensive Pt-based catalysts in fuel cells can be minimized by supporting them on high surface area carbon.

Carbon mesostructured from Korea (CMK) is one such family of OMCs [30]. Produced inside of the channels of mesostructured silicates or aluminosilicates, CMKs have specific surface areas from 1000 to 2000 m^2/g and pore volumes from 0.5 to over 1 mL/g. These materials are promising for hydrogen storage applications.

The MOF and CMK have similar behavior in hydrogen uptake capacity. CMK nanocarbons are important candidates of hydrogen uptake because of their lightweight, abundant natural precursors, and low cost [31]. Thus, CMK-3 was chosen as an ideal candidate as a support material for hydrogen storage, because they have large surface area, high chemical stability, uniform pore diameters accessible porosity, and three-dimensional conducting network [32,33]. MOFs are organometallic compounds that have a mesoporous zeotype framework with mesoporous cage and microporous windows, a big cell volume, huge surface area, and numerous unsaturated metal sites [34]. The hydrogen storage ability of these materials is related to the van der Waals interactions between their surface and hydrogen molecules [35]. It seems that the small pores in MOF play a major role on the hydrogen adsorption. The values in hydrogen adsorption capacity are close to values of other porous materials such as nanostructured carbons [31].

Therefore, the high hydrothermal stability, together with its high adsorption capacities, makes MOFs an attractive candidate for hydrogen adsorption like CMK-3 carbon. Anbia and Mandegarzad [36] prepared a MIL-101 modified with Pt/CMK. Their work shows an improvement in the hydrogen adsorption capacity after modifying the MIL-101TE with Pt (20 wt%)/CMK-3 and carbon bridge.

Metal particles dispersed in the porosity of active carbons are largely contributing to enhancing storage abilities. Numerous studies focused on this feature. Generally, hydrogen spillover was evidenced. The catalyst is supposed to trigger the H_2 dissociation, and then atomic hydrogen is assumed to diffuse deeper in the microporous network and even in between graphitic layers.

Xia *et al*. [31] studied CO_2 activation effect in ordered porous carbon CMK-3 applied in hydrogen storage. The H_2 adsorption of CMK-1 is around 1.2 wt% at 1 bar and the activated around 2% [31]. Kim *et al*. have investigated the OMCs as support materials for Pt catalysts for oxygen reduction reaction [37]. Kuppan and Selvam have studied the effect of the preparation of platinum-supported mesoporous carbon (Pt/CMK-3) as anodic catalyst for direct methanol fuel cell applications [38].

The platinum activity in adsorption of hydrogen molecules (spillover) is improved producing significant changes in hydrogen sorption properties. After Pt-CMK-3 impregnation, a loss of specific surface area and total pore volumes was observed, but at 77 K, the hydrogen uptake is better than pristine material, which have improved the hydrogen uptake that has cause enhanced 'spillover' mechanism and may promote the adsorption of molecular hydrogen on the surface of Pt nanoparticles, and also a further hydrogen diffusion into the porosity of the carbon. This material improves the hydrogen uptake capacity of CMK-3 nanometric carbon. Pt clusters dispersed on CMK-3 support of large particle size and long channel lengths possess a design in order to enhance the hydrogen uptake.

In this work, ordered porous carbon designated as CMK-3 was synthesized by replication from SBA-15 silica and then was modified with platinum in order to gain a higher hydrogen storage capacity.

Our goal was to evaluate the hydrogen storage capacities of CMK-3 replica modified with Pt nanospecies. The

approach includes synthesis and characterization of carbon-modified nanostructures along with experimental study of their adsorption capacity and storage properties.

2. MATERIAL AND METHODS

2.1. Preparation of SBA-15 template

Ordered mesoporous silica SBA-15 was prepared by using the triblock copolymer, poly(ethylene glycol)-block-poly (propylene glycol)-block-poly(ethylene glycol), ($EO_{20}PO_{70}EO_{20}$, P123-Sigma-Aldrich), as the surfactant and tetraethyl orthosilicate (Sigma-Aldrich, reagent grade 98%) as the silica source. The procedure designed is described as follows: 20 g of P123 was dissolved in a solution of HCl 1 M (400 mL) with stirring at 323 K. Then, 40 g of tetraethyl orthosilicate was added, and the resulting mixture was stirred at 323 K for 24 h. The milky mixture was transferred into a PP bottle and aged at 373 K for 72 h. The solid was separated by filtration, washed with deionized water until pH ~6. The molar composition was 1 Si:0.018 $EO_{20}PO_{70}EO_{20}$:2.08 HCl:112 H_2O. To remove the template, the material was immersed in ethanol reflux for 6 h and then calcined at 823 K in air for 6 h. The product was filtered, washed, and dried in air at 363 K [39].

2.2. Synthesis of CMK-3

Ordered porous carbon CMK-3 was synthesized via a two-step impregnation of the mesopores of SBA-15 with a solution of sucrose using an incipient wetness method. Briefly, 1.0 g of the as-prepared SBA-15 was impregnated with an aqueous solution obtained by dissolving 1.1 g of sucrose and 0.14 g of H_2SO_4 in 5.0 g of deionized water. The mixture was then dried at 373 K for 6 h and subsequently at 433 K for 6 h. The silica sample, containing partially polymerized and carbonized sucrose, was treated again at 373 K and 433 K after the addition of 0.65 g of sucrose, 90 mg of H_2SO_4, and 5.0 g of deionized water. The sucrose–silica composite was then heated at 1173 K for 4 h under nitrogen flow (20 mL/min) to complete the carbonization.

The silica template was dissolved with 5 wt% hydrofluoric acid at room temperature. The template-free carbon product thus obtained was filtered, washed with deionized water and ethanol, and dried [31].

2.3. Synthesis of Pt-CMK-3

The sample was prepared by wetness impregnation using cloroplatinic acid ($H_2PtCl_6.H_2O$-Sigma-Aldrich) as source of Pt. A solution of cloroplatinic acid in ethanol was mixed to carbon solution at ambient temperature. The solution was placed in a rotary evaporator to remove excess of ethanol at about 333 K and 60 rpm. Afterwards, the sample was dried at 373 K for 18 h. Then, the resulting material was thermally treated in a dynamic inert (N_2) atmosphere from 298 to 473 K with a slope of 10 K/min and kept at this temperature during 5 h; after that, the temperature was increased to 743 K with a slope of 10 K/min, kept 5 h at that temperature. Nitrogen flow was always 20 mL/min. The sample was treated under H_2 flow, at 773 K for 6 h with ramp rate 10 K/min. The sample was denoted as Pt-CMK-3. The percentage of Pt has been 1% with respect to carbon in the final Pt-CMK-3 material.

2.4. Characterization

The structural characteristics of the template (SBA-15) and the nanostructured carbon material (CMK-3 and Pt-CMK-3) were obtained from small angle X-ray diffraction (XRD). The XRD patterns were recorded with a Philips X'Pert PRO PANalytical diffractometer under Cu Kα radiation ($\lambda = 0.154$ nm). Measurements of N_2 (99.999%) adsorption–desorption isotherms at 77 K were carried out using a volumetric adsorption apparatus (ASAP 2020 instrument). Samples were previously degassed at 423 K for 10 h, until residual pressure was smaller than 0.5 Pa.

The transmission electron microscopy (TEM) micrographs were taken on a TEM Philips EM 301 instrument, operated at 100 kV. The elemental compositions and the formation of core-shell structure of Pt nanoparticles were identified by energy dispersive spectrometer (EDS) that is attached to a Philips EM 301 TEM instrument.

X-ray photoelectron spectra (XPS) were obtained on a MicrotechMultilb 3000 spectrometer, equipped with a hemispherical electron analyzer and MgKα ($h\nu = 1253.6$ eV) photon source. An estimated error of ±0.1 eV can be assumed for all measurements. Intensities of the peaks were calculated from the respective peak areas after background subtraction and spectrum fitting by a combination of Gaussian/Lorentzian functions. The relative surface atomic ratios were determined from the corresponding peak intensities, corrected with tabulated sensitivity factors, with a precision of ±7%. Hydrogen chemisorption characterization was performed in Micromeritics Chemisorb 2720 apparatus, equipped with a thermal conductivity detector, at room temperature and atmospheric pressure. The samples were purged with N_2 (25 mL/min) at 673 K. For pulse chemisorption analysis, samples were cooled to 295 K and titrated with H_2 pulses in a stream of N_2 until a constant output thermal conductivity detector signal indicates saturation.

Hydrogen storage isotherms at 77 K at low and high pressures (up to 10 bar) were measured using a home-made equipment calibrated appropriately. Before the hydrogen storage test, metal-doped carbons were heated under high vacuum at milder temperature in order to prevent a possible decomposition of metal nanoparticles at higher temperatures (523 K for at least 8 h. Then the samples were cooled at room temperature. For the adsorption experiments, high-purity hydrogen gas (99.9999%) was employed into the equipment. Volumetric equipment was used for hydrogen storage capacity (hydrogen physisorption) in a pressure range from 0 to 10 bar. It performed a set-up calibration of the total volume of the equipment, using a standard volume. There were no observable leaks in the instrument.

Int. J. Energy Res. 2015; **39**:128–139 © 2014 John Wiley & Sons, Ltd.
DOI: 10.1002/er

The calibration of the equipment was performed for each sample in order to obtain the volume occupied by the sample and its density. Experiments were also run in blank to determine the dead volume at 77 K. Before each experiment, the equipment is filled with gas and purged several times. To diminish the experimental error in data collection, it was calibrated with a standard sample.

3. RESULTS AND DISCUSSION

3.1. Morphological studies of samples

Figure 1 shows the typical XRD pattern for the silica template SBA-15 and the carbon CMK-3 obtained following the aforementioned procedures. The low-angle XRD pattern of SBA-15 indicates excellent structural order for the hexagonal P6mm crystallographic space group (Table I). The carbon CMK-3 obtained, by removing the silica wall after carbonization, exhibits a similar pattern relative to SBA-15. The structure of CMK-3 material, synthesized using silicate SBA-15 template, was found to be an exact negative replica of the template. The main indication of the structural transformation was the appearance on the XRD patterns of CMK-3 that was consistent with the symmetry of SBA-15 [30].

The low-angle XRD patterns of CMK-3 and the metal modified sample can be observed in Figure 1. After the incorporation of Pt, the overall pore structure is retained as indicated by the appearance of low-angle diffraction peaks (Table I). However, the signal intensity corresponding to [1 1 0] diffraction plane of the sample decreases slowly compared with the parent CMK-3. In general, the introduction of scattering material into the pores leads to an increased phase cancellation between scattering from the wall and the pore regions. The loss in intensity of CMK-3 typical Bragg reflections is due to the introduction of scattering material (Pt) into the pores [40].

Figure 2 shows the wide-angle (20°–70°) diffraction region of the samples. SBA-15 sample shows a typical XRD pattern of these mesoporous materials. CMK-3 shows two broad diffraction peaks that can be indexed as [0 0 2] and [1 0 0] diffraction for typical graphite carbons [41].

The pattern of Pt-CMK-3 shows metallic Pt signals [38], indicating a quite well reduction process. The absence of prominent reflections in case of Pt clusters indicates that no crystalline bulk material has been formed outside the pore system [42], with nanometric size and high dispersion (very broad XRD signal of Pt, Figure 2) as it can be seen in Table II. This can be ascribed to a relatively low scattering contrast between the pores and the walls of the mesoporous materials due to the formation of

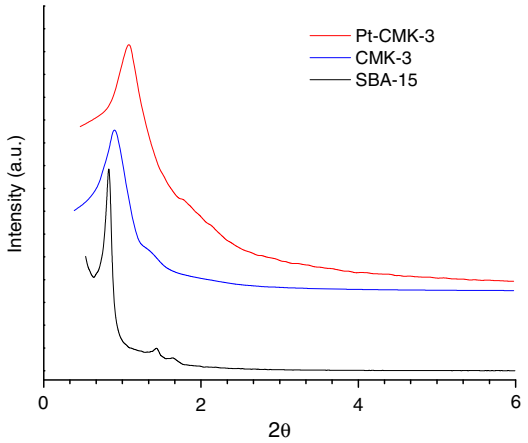

Figure 1. Small-angle X-ray diffraction patterns of SBA-15, CMK-3 and Pt-CMK-3.

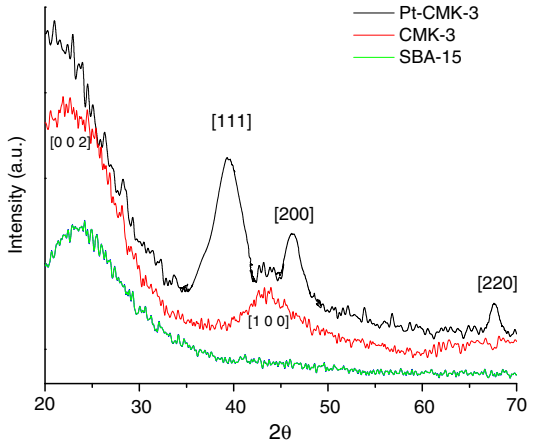

Figure 2. Wide-angle X-ray diffraction patterns of SBA-15, CMK-3 and Pt-CMK-3.

Table I. X-ray diffraction parameters of samples.

	SBA-15 [h k l]			CMK-3 [h k l]			
	[100]	[110]	[200]	[100]	[110]	[200]	
Sample	*d* (nm)			*d* (nm)			a_o (nm)
SBA-15	8.6	5.0	4.3	—	—	—	10.0
CMK-3	—	—	—	10.5	6.1	5.2	12.1
Pt-CMK-3	—	—	—	8.4	4.9	4.2	9.7

Table II. Textural and structural properties of the samples.

Sample	Area m^2/g	V_P (cm^3/g) mesoporous Volume	BJH pore diameter (nm)*	Metal cluster average size (nm)**	H_2 sorption (wt%)***
SBA-15	904	1.38	7.5	—	—
CMK-3	950	1.30	4	—	2.2
Pt-CMK-3	500	0.98	3.8	1.77	3.3

*Calculated by Barrett-Joyner-Halenda (BJH) analysis.
**Estimated by transmission electron microscopy and X-ray diffraction by Scherrer's formulae and hydrogen chemisorption.
***H_2 sorption at 10 bars and 77 K.

reduced platinum that depicts fine dispersion on CMK-3 with a narrow size distribution (Table II) [43].

While the nanomaterial area is significantly smaller with the incorporation of the metal, CMK-3's characteristic structure is maintained after the metal is within the host, in agreement with the XRD studies (Table II).

The XRD pattern analyses allow determining the crystals size of metallic particles in the samples, and the effect on the metal dispersion was obtained. The average cluster size was estimated from the width of the diffraction peaks corresponding to different [h k l] Miller index using Scherrer's formula [44].

$$d = \frac{K\lambda}{\beta\cos(\theta)} \quad (1)$$

Here d is the mean size of the ordered (crystalline) domains (the crystal average size defined as the cube root of the material volume). Furthermore, λ is the X-ray wavelength (1.54 Å), β the full width at half-maximum (in radians) of the same diffraction peak and θ the Bragg angle. The Scherrer constant, K, is a dimensionless shape factor that depends on the shape of the nanocluster (has a typical value of about 0.89), and if the clusters are not spherically shaped on the [h k l] index of the diffraction peak, the K value is 0.83 [45], although it is not this case.

For the application of Scherrer formula, were employed [1 1 1], [2 0 0] and [2 2 0] refractions plains for Pt-CMK-3. The metal particles average diameters obtained by Scherrer's formula were ~1.76 nm.

Hydrogen chemisorption was carried out to samples. The hydrogen chemisorption at room temperature was 0.19 mL/g for Pt-CMK-3: (CMK-3 did not present H_2 chemisorption), indicating that there was a few little chemical reactions or strong H_2-metal bonds and hydrogen adsorption was fully reversible. The percent of metal dispersion was 65%, and the average crystallite size of platinum was ~1.70 nm. The calculated platinum nanoparticles sizes from the computed values from XRD (see also Table II) are in concordance with TEM images and size distribution (Figure 8). Thus, it is evident that a narrow particle size distribution of 1–2 nm is obtained.

The textural properties of the samples SBA-15, CMK-3 and Pt-CMK-3 carbon were determined from nitrogen physisorption analysis (Figure 3 and Table II). The nitrogen adsorption–desorption isotherm for SBA-15 is a typical type IV curve with hysteresis loop, according to IUPAC classification, revealing the mesoporous nature of the material.

The isotherm for CMK-3 and Pt-CMK-3 samples exhibit hysteresis loops at a relative pressure range of 0.4–0.8, which can be attributed to capillary condensation–evaporation from the mesopores. The material consists of fairly uniform carbon rods (see TEM images) and higher pore volume resulting from mesopores between carbon rods. Some irregularities in channels were attributed to an incomplete filling of SBA-15 meso-tunnels with carbon precursor, from the presence of a fraction of nonlinear channels in the SBA-15. The pore size distribution of CMK-3 shows a sharp peak at 4 nm that indicates a quite regular array of nanopores.

In contrast, pore size distribution of Pt-CMK-3 shows a broad peak with a maximum at approximately 3.8 nm, which corresponds to primary mesopores. The reason of the appearance of a wide peak is the filling of pores with Pt nanoclusters and the increase of the irregularity in nanopores. Around 6 nm, an overlapped peak appears corresponding to CMK-3 pores that no fill with Pt nanoclusters. These pore size analyses were consistent with the TEM observations.

3.2. Transmission electron microscopy studies

Figure 4 shows TEM images of SBA-15 synthesized to be used as an inorganic template. An ordered mesoporous array of longitudinal nanochannels can be observed in the Figure 4 with pore diameter of 7.5 nm. Figure 5 shows TEM images of CMK-3. Ordered structure was shown to be slightly damaged by thermal treatments and exhibit well-organized pores parallel to each other. The white lines are corresponding to the mesopores generated in the space previously occupied by the walls of SBA-15 template.

Figure 6 illustrates the TEM micrographs of Pt-CMK-3. The ordered mesostructure of sample can be seen from Figure 6a and b, which indicates that the ordered structure of CMK-3 is retained after the incorporation of Pt nanoparticles. The places with darker contrast (small dark spots) could be assigned to the presence of Pt particles with a great and regular dispersion. The images indicate the fine dispersion on CMK-3 from reduced platinum, with a narrow size distribution (Figure 7) and an average diameter of ~1–2 nm within the mesopores of the framework structure CMK-3. The Pt nanoclusters sites are active sites for hydrogen adsorption, and narrow pore size distribution is important because the level of dispersion is better and the active metal area is superior. The existence of platinum inside the pore system of CMK-3 indicates an improvement in the dispersion phenomena compared with the metal only in the external surface of CMK-3.

The particle size distribution ranging from 1 to 2.5 nm indicates that metal particles are mainly present inside the pores, and the mean particle diameter was found to be close to 1.74 nm indicating that most of the particles reside inside of the pore system.

Kuppan *et al*. [38] reported that dispersion and particle size distribution of platinum nanoparticles on CMK-3 is strongly dependent on both deposition method and carbon support properties, suggesting that the reduction method with paraformaldehyde of platinum nanoparticles deposited on mesoporous carbon CMK-3 is superior to other methods of reduction, including H_2 reduction.

In this work, we show that the nature of the Pt incorporation to CMK-3 and the preparation of the Pt-CMK-3 before Pt reduction procedure (under N_2 atmosphere and

Int. J. Energy Res. 2015; **39**:128–139 © 2014 John Wiley & Sons, Ltd.
DOI: 10.1002/er

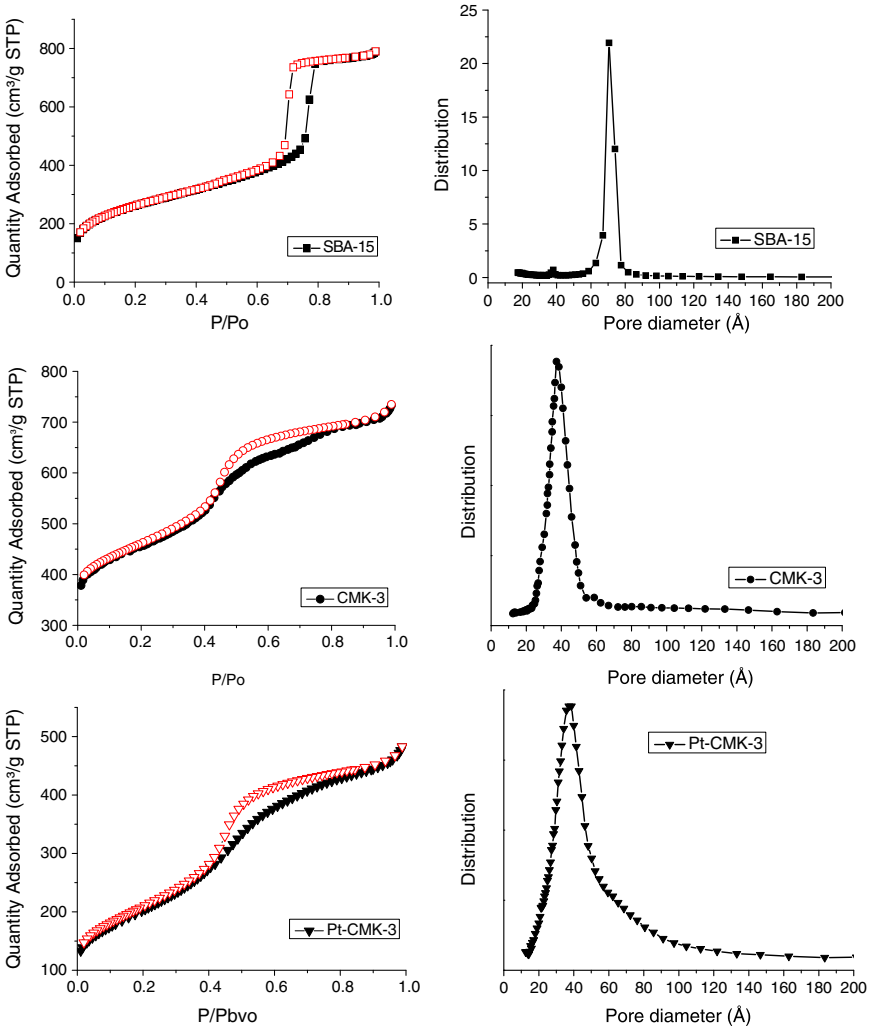

Figure 3. Nitrogen adsorption (solid symbols)–desorption isotherm (open symbols) at 77 K and pore size distribution of (a) SBA-15, (b) CMK-3, and (c) Pt-CMK-3.

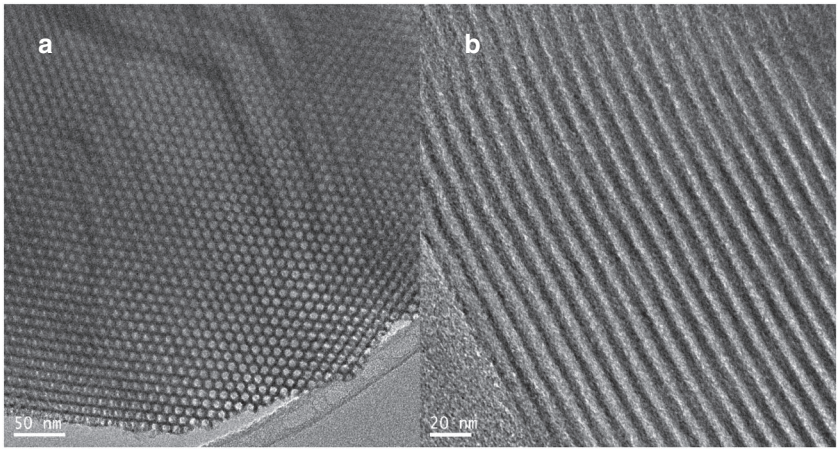

Figure 4. Transmission electron microscopy images of SBA-15. (a) [1 0 0] and (b) [1 1 0] reflection planes.

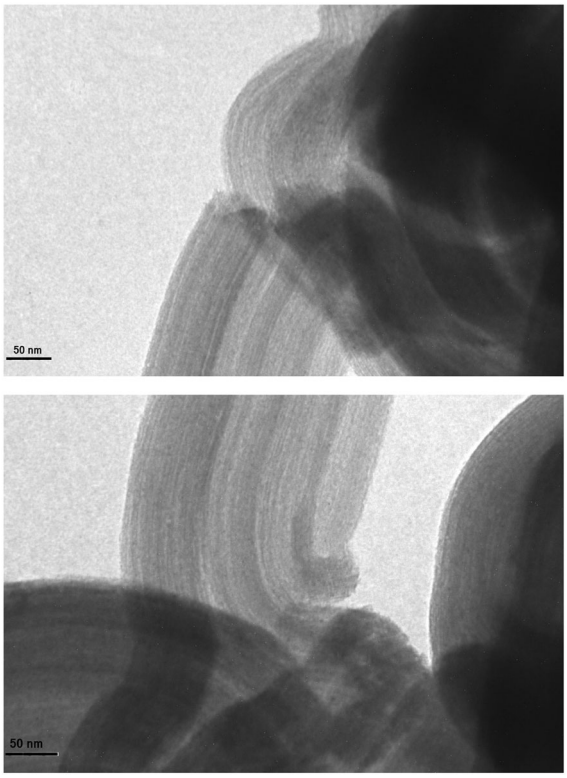

Figure 5. Transmission electron microscopy images of CMK-3.

controlled temperature elimination of the Pt precursor) influence the posterior Pt-reduced nanoparticles sizes, obtaining a narrow distribution, around 1.74 nm (Figure 7 and Table II). If the first elimination of Pt precursors-CMK-3 is obtained under oxidative atmosphere, there is more possibility of generation of larger Pt cluster. We found the same effect on iridium incorporation over SBA-16, showed in the recent work [46]. Under N_2 flow and controlled temperature desorption, the component of the Pt source elimination (cloroplatinic acid in ethanol-CMK-3) is endothermic and not oxidative, avoiding the migration and agglomeration of Pt particles after its reduction with H_2.

In order to determine the presence of Pt in the prepared Pt-CMK-3, the elemental compositions for C, O and Pt

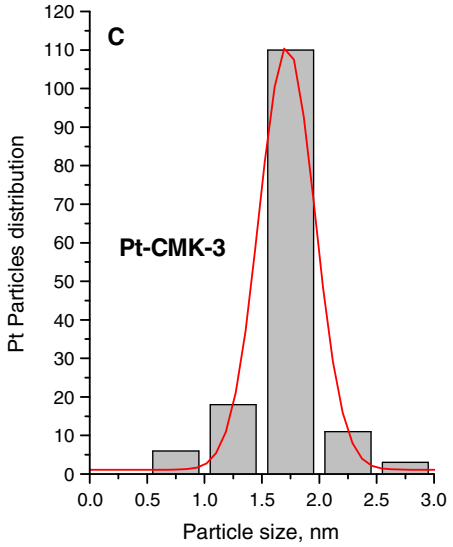

Figure 7. Histograms of PSDs measured from full images of Pt-CMK-3 shown in Figure 6a and b.

nanoparticles were carefully evaluated by EDS analysis (Figure 8). The contents of all elements were evaluated on the basis of the maps of elements collected from four spots. Thus, the average of the atomic percentage of C, O and Pt nanoclusters in Pt-CMK-3 is about 98.82%, 0.28 % and 0.9%, respectively (Table III).

3.3. X-ray photoelectron spectra characterization

The determination of the nature and oxidation state of Pt species (Pt^0, Pt^{2+} and Pt^{4+}) is normally accomplished using XPS technique and in particular by means of the Pt (4f) peak study (Figure 9). It is known that metallic Pt^0 has binding energies of 70.7–70.9 eV and 74.0–74.1 eV for $4f_{7/2}$ and $4f_{5/2}$ electrons, respectively [47]. In oxidized states, Pt^{2+} and Pt^{4+} exhibit much higher binding energies: 72.8–73.1 eV ($4f_{7/2}$) and 76.3–76.4 eV ($4f_{5/2}$) for Pt^{2+} and 74.6–74.9 eV ($4f_{7/2}$) and 78.1–78.2 eV ($4f_{5/2}$) for Pt^{4+} [48].

In this way, XPS were performed to examine the state of Pt. Metallic Pt was found to be the predominant species

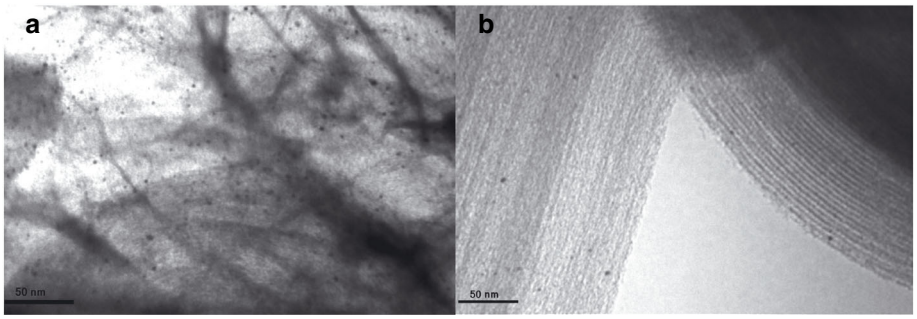

Figure 6. Transmission electron microscopy images of Pt-CMK-3.

Int. J. Energy Res. 2015; **39**:128–139 © 2014 John Wiley & Sons, Ltd.
DOI: 10.1002/er

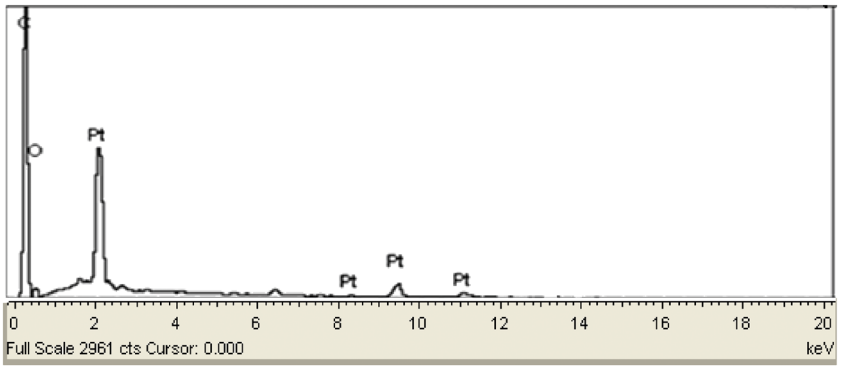

Figure 8. Energy dispersive X-ray spectrometry of Pt-CMK-3.

Table III. Energy dispersive spectrometer analysis of C, O and Pt in Pt-CMK-3. All spots (displaying wt%).

Pt-CMK-3	C	O	Pt
Spot 1	98.8	0.3	0.9
Spot 2	98.9	0.2	0.91
Spot 3	98.8	0.28	0.915
Spot 4	98.75	0.33	0.912

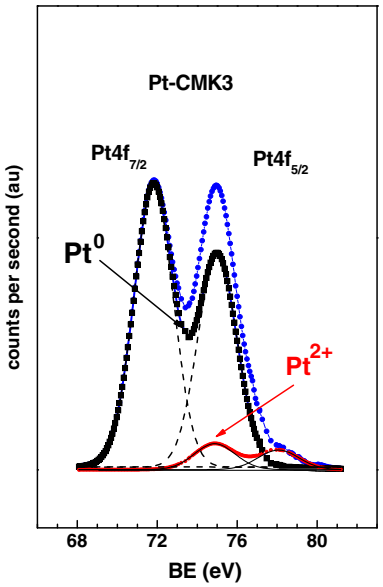

Figure 9. Core level Pt_{4f} X-ray photoelectron spectra of Pt-CMK-3.

in CMK-3, as shown in Figure 9. Spectra were resolved in two pairs of peaks. The main peaks in all spectra are doublets containing a high energy band, Pt $4f_{5/2}$, and a low energy band, Pt $4f_{7/2}$, which appeared at 75.1 and 71.8 eV, respectively, indicating that deposited Pt is metallic (Table IV). It must be noted that the observed shift of the Pt^0 peak to slightly higher binding energies is in accordance to the known effect for small particle sizes, as reported by Roth *et al*. [48] and Takasu *et al*. [49] or for charge transfer between platinum and carbon reported by Aricò *et al*. [50]. The second pair of Pt signals appears around 74.9 and 77.1 eV and has been reported to be due to presence of PtO or PtO_2 [46, 51]. In Table IV, we can see the chemical composition obtained by XPS of Pt-CMK-3 and peak position for C, O and Pt.

Following XPS analysis, the Pt concentration at 50 Å of depth was 0.38 wt%, whereas using ICP and EDS analysis (Figure 8), indicating a nominal Pt = 0.9 wt% on Pt-CMK-3 allowed us to suggest that the majority of Pt^0 is inside the nanostructure of CMK-3 sample. Moreover, about 80 wt% of oxygen is on external surface of CMK, with the corresponding lower amount of unreduced Pt species ($Pt^{2,4+}$).

3.4. Hydrogen uptake measurements

The capacity of hydrogen storage was evaluated at low and high pressures and cryogenic temperatures (77 K).

The experimental data were fitted by Freundlich isotherm [52] that is a purely empirical formula for gaseous adsorbates. The Freundlich model is described by the following equation:

$$Q = K_F P_n^{\frac{1}{n}} \quad (2)$$

Table IV. Energy binding (eV) and chemical composition (at%) of Pt-CMK-3.

Sample	C1s	O1s	Pt $4f_{7/2}$	C (at%)	O (at%)	Pt (at%)
Pt-CMK-3	284.8 (86)	531.8 (35)	71.8 (89)	99.47	0.6	0.03
	286.4 (14)	533.7 (65)	74.9 (11)			

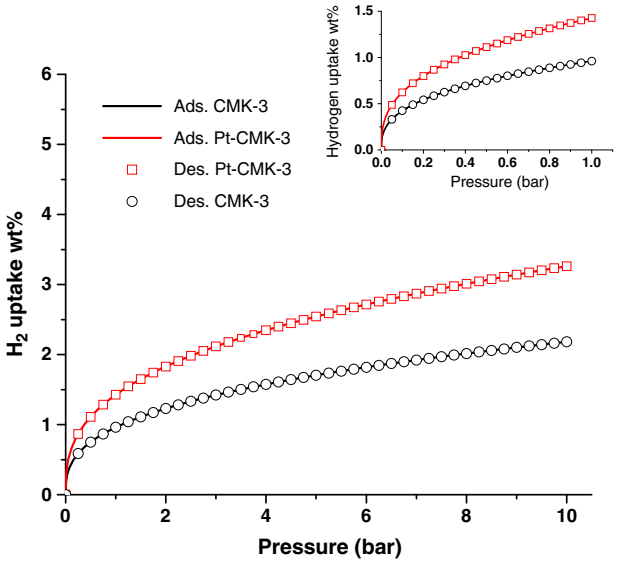

Figure 10. H_2 adsorption–desorption isotherms of CMK-3 and Pt-CMK-3.

where Q is the quantity adsorbed per unit mass of adsorbent, P is the pressure of adsorbate, and K_F and n are empirical constants, called Freundlich constants, for each adsorbent–adsorbate pair at a given temperature. The K_F is a measurement of the adsorption, and n is a measure of the adsorption intensity [52]. As the temperature increases, the constants K_F and n change to reflect the empirical observation that the quantity adsorbed rises more slowly and higher pressures are required to saturate the surface.

The experimental data were fitted to the Freundlich equation using least-squares nonlinear regression for arbitrary fit functions and minimizing the objective function employing Levenberg–Marquardt method. The fitting accuracy was $R^2 = 0.98$.

Figure 10 shows the adsorption–desorption isotherms of hydrogen at 77 K on CMK-3 and Pt-CMK-3 samples at a range of pressures (0–10 bar). The inset of this figure shows the behavior at low pressures (0–1 bar).

At low and high pressures, the amount of hydrogen uptake is higher in Pt-CMK-3 sample than CMK-3 sample (Table II). We employed the term 'uptake' as storage (carbon like a sponge); thus, the process is completely reversible, and the curve becomes in the same place, because every point returns to initial values.

The proposed mechanism for hydrogen storage in Pt-CMK-3 agreed with Kim *et al.* [53]. There are at least two ways in the process of physisorption of hydrogen on the Pt-CMK-3 surface. The molecules of hydrogen spill over onto the CMK-3 nano/micropores and adsorbed onto nanometric metal clusters. It was found that the hydrogen adsorption was fully reversible [53], indicating that there was no chemical reaction or strong bonds between hydrogen and metal nanocluster or CMK-3 framework.

Therefore, a dipole-induced model is proposed. The first layer of hydrogen molecules could be reacted with the metal cluster because of high oxidation metal capacity interacting like as dihydrogen complex [49], but the amount of this initial interaction is insignificant. The second layer of hydrogen molecules is physically adsorbed by dipole-induced interaction. Hydrogen molecules are basically nonpolar, but the strong interaction of the metal particles leads to the dipole-inducing effects of the hydrogen molecules. The third layer and any upper layer of hydrogen molecules could interact with metal cluster by the same mechanism, but the force of the dipole-induced bond is weakly and reduces when the distance to the surface increases. This mechanism can be applied at higher pressure consequently; Pt-CMK-3 adsorbs more amount of hydrogen than the carbon at higher pressures.

4. CONCLUSIONS

We have shown that a promising hydrogen storage material can be obtained by ordered porous carbon CMK-3 modified with Pt nanoparticles, which was synthesized by replication using SBA-15 as template, and incorporation of metal was carried out by wetness impregnation, supported by XRD and N_2 isotherm studies. The CMK-3 modified with Pt presents a better capacity for hydrogen uptake than the nanometric carbon CMK-3. The enhanced activity and the superior performance of Pt/CMK-3 is due to improved dispersion of uniform platinum nanoparticles as well as better utilization of the support, which probably was originate of a high surface area and pore volume, which allows a large dispersion of Pt. The study also demonstrates that optimized carbon supports can offer significant improvement by way of lowering the noble metal loading.

The nanoparticles of Pt in Pt-CMK-3 have a smaller size (~1.7 nm average, obtained by XRD, TEM and H_2 chemisorptions) and a quite well dispersion, and the

Int. J. Energy Res. 2015; **39**:128–139 © 2014 John Wiley & Sons, Ltd.
DOI: 10.1002/er

occlusion of nanopores of the carbon framework is lower, although Pt is almost in the nanoporous of CMK-3 according to the XPS and ICP-EDS analyses.

This indicates the better hydrogen adsorption of the Pt-CMK-3 sample than CMK-3 carbon. A hydrogen storage mechanism on metal/carbon surfaces was proposed. We can conclude this work indicating that CMK-3 hydrogen storage capacity was increased by addition of metal clusters. Also hydrogen storage behaviors onto Pt-CMK-3 can be optimized by controlling the metal cluster size and dispersion and also increasing the carbon specific surface area.

ACKNOWLEDGEMENTS

JMJ holds a Conicet fellowship, and MGC and OAA are Conicet researchers. The authors thank the CONICET Argentina, PIP No. 112-200801-00388 (2009–2013). The authors are very grateful to Drs. J. L. García Fierro and H. Falcon for XPS and TEM-EDS characterizations performed in ICP-CSIC, Madrid.

REFERENCES

1. Cho SJ, Choo K, Kim DP, Kim JW. H_2 sorption in HCl-treated polyaniline and polypyrrole. *Catalysis Today* 2007; **120**:336–340.
2. White CM, Steeper RR, Lutz AE. The hydrogen-fueled internal combustion engine: a technical review. *International Journal of Hydrogen Energy* 2006; **31**(10): 1292–1305.
3. Jurczyk MU, Kumar A, Srinivasan S, Stefanakos E. Polyaniline-based nanocomposite materials for hydrogen storage. *International Journal of Hydrogen Energy* 2007; **32**(1):1010–1015.
4. Schlapbach L, Züttel A. Hydrogen-storage materials for mobile applications. *Nature* 2001; **414**:353–358.
5. Gadiou R, Saadallah SE, Piquero T, David P, Parmentier J, Guterl CV. The influence of textural properties on the adsorption of hydrogen on ordered nanostructured carbons. *Microporous and Mesoporous Materials* 2005; **79**:121–128.
6. Fang BZ, Zhou HS, Honma I. Ordered porous carbon with tailored pore size for electrochemical hydrogen storage application. *Journal of Physical Chemistry B* 2006; **110**:4875–4880.
7. Guterl CV, Frackowiak E, Jurewicz K, Friebe M, Parmentier J, Béguin F. Electrochemical energy storage in ordered porous carbon materials. *Carbon* 2005; **43**:1293–1302.
8. Yang ZX, Xia YD, Sun XZ, Mokaya R. Preparation and hydrogen storage properties of zeolite-templated carbon materials nanocast via chemical vapor deposition: effect of the zeolite template and nitrogen doping. *Journal of Physical Chemistry B* 2006; **110**:18424–18431.
9. Saha D, Deng S. Synthesis, characterization and hydrogen adsorption in mixed crystals of MOF-5 and MOF-177. *International Journal of Hydrogen Energy* 2009; **34**:2670–2678.
10. Klyamkin SN, Chuvikov SV, Maletskaya NV, Kogan EV, Fedin VP, Kovalenko KA, Dybtsev DN. High-pressure hydrogen storage on modified MIL-101 metal–organic framework. *International Journal of Energy Research* 2014. doi:10.1002/er.3175.
11. Moussa G, Moury R, Demirci UB, Şener T, Miele P. Boron-based hydrides for chemical hydrogen storage. *International Journal of Energy Research* 2013; **37**: 825–842.
12. Liang M, Luo B, Zhi L. Application of graphene and graphene-based materials in clean energy-related devices. *International Journal of Energy Research* 2009; **33**:1161–1170.
13. Kajiura H, Tsutsui S, Kadono K, Kakuta M, Ata M, Murakami Y. Hydrogen storage capacity of commercially available carbon materials at room temperature. *Applied Physics Letters* 2003; **82**:1105–1107.
14. Mandoki NT, Dentzer J, Piquero T, Saadallah S, David P, Guterl CV. Hydrogen storage in activated carbon materials: role of the nanoporous texture. *Carbon* 2004; **42**:2744–2747.
15. Züttel A, Sudan P, Mauron P, Kiyobayashi T, Emmenegger C, Schlapbach L. Hydrogen storage in carbon nanostructures. *International Journal of Hydrogen Energy* 2002; **27**:203–212.
16. Hirscher M, Becher M. Hydrogen storage in carbon nanotubes. *Journal of Nanoscience and Nanotechnology* 2003; **3**:3–17.
17. Ansón A, Callejas MA, Benito AM, Maser WK, Izquierdo MT, Rubio B, *et al.* Hydrogen adsorption studies on single wall carbon nanotubes. *Carbon* 2004; **42**:1243–1248.
18. Pan WY, Zhang XF, Li S, Wu DH, Mao ZQ. Measuring hydrogen storage capacity of carbon nanotubes by high-pressure microbalance. *International Journal of Hydrogen Energy* 2005; **30**:719–722.
19. Tibbetts GG, Meisner GP, Olk CH. Hydrogen storage capacity of carbon nanotubes, filaments, and vapor-grown fibers. *Carbon* 2001; **39**:2291–2301.
20. Browning DJ, Gerrard ML, Lakeman JB, Mellor IM, Mortimer RJ, Turpin MC. Studies into the storage of hydrogen in carbon nanofibers: proposal of a possible reaction mechanism. *Nano Letters* 2002; **2**(3):201–205.
21. Lueking AD, Yang RT, Rodriguez NM, Baker RTK. Hydrogen storage in graphite nanofibers: effect of synthesis catalyst and pretreatment conditions. *Langmuir* 2004; **20**(3):714–721.

22. Smith MR, Bittner EW, Shi W, Johnson JK, Bockrath BC. Chemical activation of single-walled carbon nanotubes for hydrogen adsorption. *Journal of Physical Chemistry B* 2003; **107**:3752–6370.
23. Blackman JM, Patrick JW, Arenillas A, Shi W, Snape CE. Activation of carbon nanofibres for hydrogen storage. *Carbon* 2006; **44**:1376–1385.
24. Ryoo R, Joo SH, Jun S. Synthesis of highly ordered carbon molecular sieves via template-mediated structural transformation. *Journal of Physical Chemistry B* 1999; **103**:7743–7746.
25. Joo SH, Jun S, Ryoo R. Synthesis of ordered mesoporous carbon molecular sieves CMK-1. *Microporous ann Mesoporous Materials* 2001; **44–45**:153–158.
26. Jun S, Joo SH, Ryoo R, Kruk M, Jaronice M, Liu Z, *et al.* Synthesis of new, nanoporous carbon with hexagonally ordered mesostructure. *Journal of American Chemical Society* 2000; **122**:10712–10713.
27. Singer JP, Mayergoyz A, Portet C, Schneider E, Gogotsi Y, Fischer JE. Enhanced volumetric hydrogen storage capacity of porous carbon powders by forming peels or pellets. *Microporous and Mesoporous Materials* 2008; **116**:469–472.
28. Poirier E, Chahine R, Bose TK. Hydrogen adsorption in carbon nanostructures. *International Journal of Hydrogen Energy* 2001; **26**:831–835.
29. Giraudet S, Zhu Z. Hydrogen adsorption in nitrogen enriched ordered mesoporous carbons doped with nickel nanoparticles. *Carbon* 2011; **49**:398–405.
30. Yang H, Zhao D. Synthesis of replica mesostructures by nanocasting strategy. *Journal of Material Chemistry* 2005; **15**:1217–1231.
31. Xia K, Gao Q, Wu C, Song S, Ruan M. Activation, characterization and hydrogen storage properties of the mesoporous carbon CMK-3. *Carbon* 2007; **45**:1989–1996.
32. Anbia M, Ghaffari A. Adsorption of phenolic compounds from aqueous solutions using carbon nanoporous adsorbent coated with polymer. *Applied Surface Science* 2009; **255**:9487–9492.
33. Anbia M, Parvin Z. Desulfurization of fuels by means of a nanoporous carbon adsorbent. *Chemical Engineering Research and Design* 2011; **89**:641–647.
34. Hong DY, Hwang YK, Serre C, Ferey G, Chang JS. Porous chromium terephthalate MIL-101 with coordinatively unsaturated sites: surface functionalization, encapsulation, sorption and catalysis. *Advanced Functional Materials* 2009; **19**:1537–1552.
35. Hirscher M, Panella B, Schmitz B. Micropor. *Microporous and Mesoporous Materials* 2010; **129**:335–339.
36. Anbia M, Mandegarzad S. Enhanced hydrogen sorption on modified MIL-101 with Pt/CMK-3 by hydrogen spillover effect. *Journal of Alloys and Compounds* 2012; **532**:61–67.
37. Kim N, Yeong Cheon J, Hyung Kim J, Seong J, Park J, Joo S, Kwon K. Impact of framework structure of ordered mesoporous carbons on the performance of supported Pt catalysts for oxygen reduction reaction. *Carbon* 2014; **72**:354–364.
38. Kuppan B, Selvam P. Platinum-supported mesoporous carbon (Pt/CMK-3) as anodic catalyst for direct methanol fuel cell applications: the effect of preparation and deposition methods. *Progress in Natural Science: Materials International* 2012; **22**(6):616–623.
39. Meynen V, Cool P, Vansant EF. Verified syntheses of mesoporous materials. *Microporous and Mesoporous Materials* 2009; **125**:170–223.
40. Huwe H, Fröba M. Iron (III) oxide nanoparticles within the pore system of mesoporous carbon CMK-1: intra-pore synthesis and characterization. *Microporous and Mesoporous Materials* 2003; **60**:151–158.
41. Suryavanshi U, Iijima T, Hayashia A, Hayashi Y, Tanemura M. Fabrication of ZnO nanoparticles confined in the channels of mesoporous carbon. *Chemical Engeneering Journal* 2012; **179**:388–393.
42. Gómez Costa MB, Juárez JM, Martínez ML, Beltramone AR, Cussa J, Anunziata OA. Synthesis and characterization of conducting polypyrrole/SBA-3 and polypyrrole/Na-AlSBA-3 composites. *Material Reseach Bulletin* 2013; **48**:661–667.
43. Veena Gopalan E, Malini KA, Santhoshkumar G, Narayanan TN, Joy PA, Al-Omari IA, Sakthi Kumar D, Yoshida Y, Anantharaman MR. Template-assisted synthesis and characterization of passivated nickel nanoparticles. *Nanoscale Research Letters* 2010; **5**:889–897.
44. Langford JI, Wilson AJC. Scherrer after sixty years: a survey and some new results in the determination of crystallite size. *Journal of Applied Crystallography* 1978; **11**:102–113.
45. van Huis MA, van Veen A, Schut H, Eijt SWH, Kooi BJ, De Hosson JTM. Structural properties of Au and Ag nanoclusters embedded in MgO. *Nuclear Instruments and Methods in Physics Research Section B* 2002; **191**:442–446.
46. Ledesma BC, Vallés VA, Rivoira LP, Martínez ML, Anunziata OA, Beltramone AR. Hydrogenation of tetralin over Ir catalysts supported on titania-modified SBA-16. *Catalysis Letters* 2014; **144**:1–13.
47. Contour JP, Mouvier G, Hoogewijs M, Leclere C. X-ray photoelectron spectroscopy and electron microscopy of PtRh gauzes used for catalytic oxidation of ammonia. *Journal of Catalysis* 1977; **48**:217–228.
48. Roth C, Goetz M, Fuess H. Synthesis and characterization of carbon-supported PteRueWOx catalysts by spectroscopy and diffraction methods. *Journal of Applied Electrochemistry* 2001; **31**:793–798.

Int. J. Energy Res. 2015; **39**:128–139 © 2014 John Wiley & Sons, Ltd.
DOI: 10.1002/er

49. Takasu Y, Unwin R, Tesche B, Bradshaw AM, Grunze M. Photoemission from palladium particle arrays on an amorphous silica substrate. *Surface Science* 1978; **77**:219–232.
50. Aricò AS, Antonucci V, Giordano N, Shukla AK, Ravikumar MK, Roy A, Barman SR, Sarma DD. Methanol oxidation on carbon-supported platinum-tin electrodes in sulfuric acid. *Journal of Power Sources* 1994; **50**:295–309.
51. Kim KS, Winograd N, Davis RE. Electron spectroscopy of platinum-oxygen surfaces and application to electrochemical studies. *Journal of American Chemical Society* 1971; **93**:6296–6297.
52. Zeinaldi F, Ghoreyshi AA, Najafpour GD. Adsorption of dichloromethane from aqueous phase using granular activated carbon: isotherm and breakthrough curve measurements. *Middle East Journal science Reserch* 2010; **5**(4):191–198.
53. Kim B-J, Park S-J. Optimization of the pore structure of nickel/graphite hybrid materials for hydrogen storage. *International Journal of Hydrogen Energy* 2011; **36**:648–653.